CrystEngComm

PAPER

View Article Online
View Journal | View Issue

Cite this: *CrystEngComm*, 2016, **18**, 7972

Structural response to desolvation in a pyridyl-phenanthrene diarylethene-based metal–organic framework†

Ian M. Walton,[a] Jordan M. Cox,[a] Travis B. Mitchell,[a] Nicholas P. Bizier[b] and Jason B. Benedict*[a]

Received 15th August 2016,
Accepted 27th September 2016

DOI: 10.1039/c6ce01783e

www.rsc.org/crystengcomm

A phenanthrene-based diarylethene linker with linear pyridyl connectivity, 4,4′-(9,10-bis(2,5-dimethylthiophen-3-yl)phenanthrene-2,7-diyl)dipyridine linker (**TPDPy**) was prepared and subsequently used to synthesize an air-stable metal–organic framework, **UBMOF-3** ($Zn_3(BDC)_3(TPDPy)_1(DMF)_{1.5}$, BDC = 1,4-benzenedicarboxylate, DMF = *N*,*N*-dimethylformamide). Upon irradiation with ultraviolet light, this photo-responsive framework, composed of terephthalate, **TPDPy**, and zinc pinwheels, exhibits strong linear dichroism consistent with the crystal structure. Activation (desolvation) of the crystal leads to a significant change in the crystal structure that improves the ability to crystallographically resolve the photochromic linker.

Introduction

Permanently porous crystalline solids, such as metal–organic frameworks (MOFs), zeolitic imidazole frameworks (ZIFs), and porous coordination polymers (PCPs), have received considerable attention in recent years due to their potential applications in chemical separations, carbon dioxide sequestration, and low-pressure fuel storage.[1–5] While the accessible void space and high surface area are ideal for guest storage, the selective release of the confined guest would greatly improve the performance of these materials in a variety of applications, most notably drug delivery.[6]

The functionalization of frameworks to introduce an active moiety into the lattice of the framework has gained considerable interest in recent years.[7–12] The incorporation of a photochromic moiety into a framework (MOFs, ZIFs, and PCPs) can provide external control over the void space through irradiation of the material with a specific wavelength of light, enabling the selective release of a loaded guest.[13–15] The benefits of light based control over other potential routes of control such as heat, pH, or current, are both the minimal interaction of the stimulus with the rest of the system as well as the potential to achieve high spatial and temporal control.[16] Photochromic technologies may also be used as energy harvesting and energy storage materials.[17–21]

A number of photochromic and photo-responsive frameworks have been reported to date, many based upon the photoactive azobenzene moiety.[22–24] Diarylethene (DAE)-based photoactive MOFs remain an attractive alternative given the strong colorimetric response that accompanies the ring-opening/closing photochemical reaction found in these systems.[25–28] Herein we report **UBMOF-3**, an air-stable metal–organic framework that utilizes a photo-responsive phenanthrene-based DAE linker with pyridyl connectivity (Fig. 1). The synthesis, structural reorganization upon activation, and

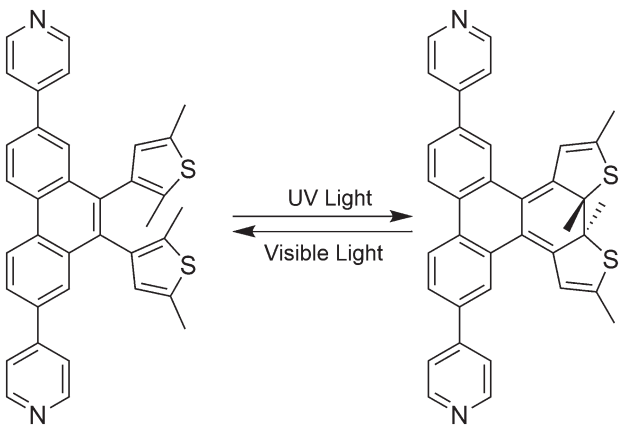

Fig. 1 Chemical structures of the ring-opened (left) and -closed (right) forms of the photochromic MOF linker, **TPDPy**.

[a] *Department of Chemistry, University at buffalo, The State University of New York, Buffalo, New York, 14260-3000, USA. E-mail: jbb6@buffalo.edu*
[b] *Department of Natural Sciences, Daemen College, Amherst, New York, 14226, USA*

† Electronic supplementary information (ESI) available: Full Gaussian09 citation, additional calculation data, single-crystal spectroscopy, polarized light images, and crystallographic data tables. CCDC 1477423–1477424 contains the supplementary crystallographic data for this paper. For ESI and crystallographic data in CIF or other electronic format see DOI: 10.1039/c6ce01783e

photo-responsive nature of the linker and framework are discussed.

Experimental

Synthesis

All starting materials, except as noted, were purchased from commercial sources and used as received. 3,3′-(2,7-Dibromo-9,10-phenanthrenediyl)bis(2,5-dimethylthiophene) (TPDBr) was synthesized using a previously reported procedure.[26]

Synthesis of 4,4′-(9,10-bis(2,5-dimethylthiophen-3-yl)-phenanthrene-2,7-diyl)dipyridine (**TPDPy**): to a 100 mL Schlenk tube was added TPDBr (0.176 g, 0.317 mmol), 4-pyridyl boronic acid (0.4668 g, 3.798 mmol), and $Na_3PO_4 \cdot 12H_2O$ (0.6014 g, 1.583 mmol) along with 7 mL of toluene, 7 mL of water, 4 mL of methanol and 2 drops of Aliquot 336. Three equivalents of 4-pyridyl boronic acid was initially added, with one equivalent added each subsequent day for three more days under nitrogen flow. The biphasic solution was taken through three freeze/pump/thaw cycles. Under strong nitrogen flow, 3 mg of $Pd(PPh_3)_4$ was added, and the reaction was taken through an additional freeze/pump/thaw cycle. The vessel was back filled with nitrogen and refluxed at 100 °C for 6 days. Upon cooling to room temperature the aqueous phase was extracted with diethyl ether (2 × 10 mL). The combined organic phases were washed with saturated brine solution (2 × 15 mL). The solvent was removed under reduced pressure *via* rotary evaporation. The product was isolated by column chromatography; 100% ethyl acetate to 95% ethyl acetate/5% methanol. 0.0653 g of product was recovered (37% yield). ^{1}H NMR ($CDCl_3$, 500 MHz) δ 8.91 (d, 2H, J = 10 Hz), 8.70 (bs, 4H), 7.99 (s, 2H), 7.96 (d, 2H, J = 15 Hz), 7.55 (t, 4H, J = 5 Hz), 6.41 (s, 1H), 6.37 (s, 1H), 2.42 (s, 3H), 2.40 (s, 2H), 2.09 (s, 3H), 2.04 (s, 3H); HRMS EI calculated for $C_{36}H_{28}N_2S_2$ 552.1688 found m/z 552.16797.

Synthesis of **UBMOF-3**: to a 15 mL thick-walled reaction vessel was added **TPDPy** (0.005 g, 0.009 mmol), terephthalic acid (0.003 g, 0.018 mmol), $Zn(NO_3)_2 \cdot 6H_2O$ (0.0054 g, 0.018 mmol), and 15 mL of *N*,*N*-dimethylformamide. The solution was heated to 85 °C for 24 hours, then cooled to room temperature. Thin pale yellow plates of **UBMOF-3** co-precipitated with a colourless cubic phase found to be MOF-5.[29] The formula of the **UBMOF-3** framework, excluding void space contents was determined to be $(Zn_3(BDC)_3(TPDPy)_1(DMF)_{1.5})$. The crystals of **UBMOF-3** were mechanically separated and analysed by single crystal X-ray diffraction (SCXRD) and single crystal UV/vis spectroscopy. Several **UBMOF-3** single crystals were activated under high vacuum for 48 hours to remove the DMF guest solvent. Crystal structures of the activated crystals revealed a new structure, **UBMOF-3a**. The formula of the **UBMOF-3a** framework, excluding void space contents, was determined to be $(Zn_3(BDC)_3(TPDPy)_1)$. To assess the relative stability of **UBMOF-3a** crystals under ambient conditions, several single crystals were allowed to rest on the benchtop uncovered for a period of 5 days. After this time, the SCXRD measurements confirmed single crystallinity had been retained.

Single crystal X-ray diffraction

X-ray diffraction data on **UBMOF-3**, and **UBMOF-3a** were collected using a Bruker SMART APEX2 CCD diffractometer installed at a rotating anode source (MoKα radiation, λ = 0.71073 Å), and equipped with an Oxford Cryosystems nitrogen gas-flow apparatus. The data were collected by the rotation method with 0.5° frame-width (ω scan) and 90 s exposure time per frame. Two sets of data (360 frames in each set) were collected for each compound, nominally covering complete reciprocal space. Using Olex2,[30] the structures were solved with the ShelXS structure solution program[31] using direct methods and refined with the ShelXL refinement package using least-squares.[32] The structures were refined by full-matrix least squares against F^2. In **UBMOF-3**, the **TPDPy** linker resides on a crystallographic center of inversion and likely exhibits numerous conformations (none of which possess a center of inversion). Given the extensive disorder only the biphenyl portion of the linker could be reliably refined and included in the final model. The occupancy of the DMF molecule in **UBMOF-3** was freely refined and determined to be 0.7503(12). In **UBMOF-3a**, **TPDPy** also resides on a crystallographic center of inversion; however, the compression of the lattice reduces the number of conformations enabling additional atoms within the phenanthrene and thiophene portions of the linker to be reliably refined. In both structures, the thermal parameters of strongly disordered atoms, generally within the phenanthrene portion of the molecule, were refined isotropically. In some instances, light constraints were necessary (SADI and EAPD) to ensure chemically reasonable geometries and thermal parameters. The SADI command restrains two or more interatomic distances to be equivalent within an effective range. The EADP command constrains the thermal displacement parameters of two or more atoms to be the same. Solvent masks were used to account for the heavily disordered solvent molecules residing in the pores and channels of the structures that could not be refined.

Spectroscopy

UV-vis spectra of the free **TPDPy** linker were measured in methanol (9.74×10^{-5} M). The solution was irradiated with white light through a 495 nm long pass filter to ensure maximum conversion to the "open" isomer. Another spectrum was taken following irradiation of the sample with 365 nm light supplied with a Thorlabs M365F1 fibre-coupled diode for 10 min. The spectra were collected using an Ocean Optics spectrometer (Model USB4000) and processed using the SpectraSuite software package.

Computational methods

The rotational energy calculation was performed on **TPDPy** using the Gaussian 09 suite of programs[33] using density

functional theory (DFT) methods with the dispersion-corrected hybrid functional ωB97XD from Head-Gordon and coworkers[34] and a 6-31G(d) basis set. The molecule was geometry optimized in its open form, and a relaxed potential energy surface scan was employed to determine the energies of the various rotational isomers. The dihedral angle, which defines the rotation of one thiophene ring, was changed incrementally by 2° and held constant at each step while the remainder of the molecule was allowed to geometrically relax.

Results and discussion

Several DAE MOFs containing linkers with pyridyl binding groups have been reported; however, in all cases the pyridyl groups are directly attached to the photoactive thiophene groups resulting in the photoresponsive group being built into the backbone of the framework.[25,27,35] **TPDPy** is the first pyridyl-based DAE MOF linker in which the photoresponsive thiophene groups are attached as a side group on the phenanthrene backbone. This design allows the photoactive pendant groups to protrude into the MOF void space and undergo photochemically-driven structural reorganization with fewer geometric constraints than might exist for photoactive groups built into the backbone.

An analysis of the potential energy surface arising from rotation of the phenanthrene–thiophene bond reveals the presence of four local minima for the ring-open molecule (Fig. 2, full scale Fig. S1†). These minima correspond to two *anti-parallel* geometries (*anti*) and two *parallel* geometries (*para*), similar to what was observed in our previous work on related DAE linkers.[28,36] Substitution at the 5-position of the thiophene ring with a methyl group instead of a phenyl ring, as in the case of **TPDPy**, had a minimal impact on the energetic barriers between the anti and para rotamers (Fig. S2†). This substitution does, however, affect the relative energies of the atropisomers as all four minima are separated in energy by less than 1 kcal mol^{-1}. It is also worth noting that the only photoactive conformer, the *anti* rotamer in which the distance between the reactive carbon atoms is less than 4.2 Å,[37] was one of the lowest energy minima on the potential energy surface as opposed to one of the highest energy minima in the case of the phenyl-substituted derivative (Fig. S2†).

Crystal structures

UBMOF-3 crystallizes in the centrosymmetric space group *C*2/*c*. The structure consists of two-dimensional sheets composed of terephthalate linkers that connect zinc pinwheel metal centres and pillaring **TPDPy** linkers (Fig. 3).[38] The rigid backbone of the **TPDPy** linker provides linear connectivity between metal centres while effectively separating the photochromic functionality from the backbone of the framework structure. The presence of multiple rotational isomers of the **TPDPy** linker within the **UBMOF-3** structure leads to strong disorder resulting in the inability to successfully resolve the thiophene pendant groups of the DAE moiety. Further disorder was observed in the coordinated DMF molecules at each end of the zinc pinwheel SBU.

Activation of **UBMOF-3** to **UBMOF-3a** resulted in a large change in the unit cell parameters and structure of the framework (Table 1). Both structures contain solvent accessible void space and channels that run parallel to the *b*- and *c*-axes. Notably, upon conversion to the **UBMOF-3a** structure, the ability to resolve the **TPDPy** linker was dramatically improved. The loss of the DMF that was coordinated to the zinc metal centre was also observed. The reorientation of the pillaring **TPDPy** linker resulted in a significant change in the unit cell, specifically a decrease in the *a*-axis by approximately 20%, and a decrease in β by approximately 11°. While the reorientation of **TPDPy** in **UBMOF-3a** improved the ability to crystallographically resolve the linker, the photo-active thiophene groups remained disordered over two positions. The ability to resolve these pendant groups is a marked improvement over our previous DAE-based frameworks that contain similar photoactive groups.[26,28]

An overlay of the asymmetric units of **UBMOF-3** and **UBMOF-3a** (Fig. 4) illustrates the pronounced change in the orientation of the pillaring **TPDPy** linker. The zinc pinwheel and corresponding terephthalate linkers are nearly identical between the two species. The shift in the **TPDPy** linker may be attributed to the loss of the previously coordinated DMF

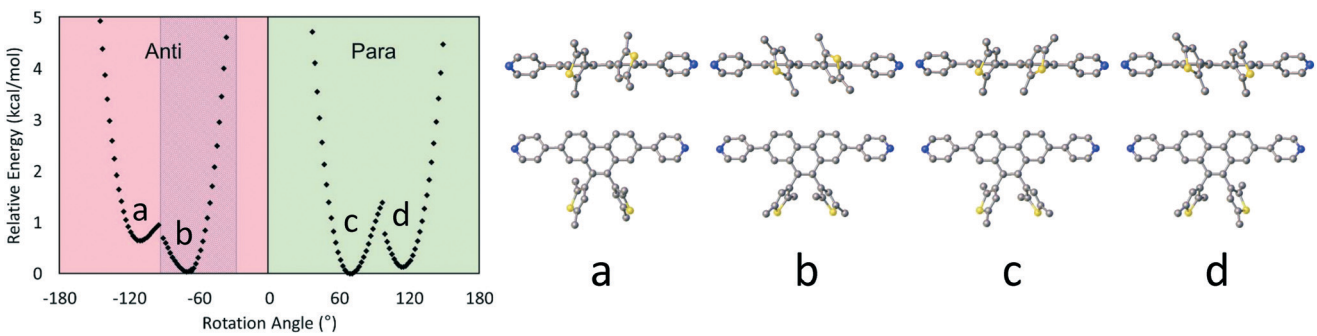

Fig. 2 Calculated potential energy surface for the dihedral rotation of one thiophene ring of **TPDPy** (left) and two views of the optimized structures for each of the four energetic minima (a–d, right). The shaded region in the graph corresponds to molecular geometries that should exhibit photochemical activity.

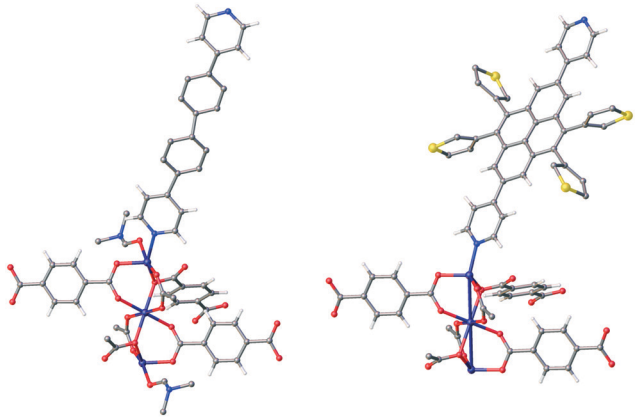

Fig. 3 Expanded asymmetric unit of **UBMOF-3** (left) and **UBMOF-3a** (right). Only the major component of the disordered **TPDPy** linker in **UBMOF-3** is shown for clarity. Several carbon atoms and the thiophene rings in **UBMOF-3** were not refined and do not appear in the model (see Experimental section). Atom colours: carbon (grey), nitrogen (blue), oxygen (red), sulphur (yellow), zinc (purple) and hydrogen (white).

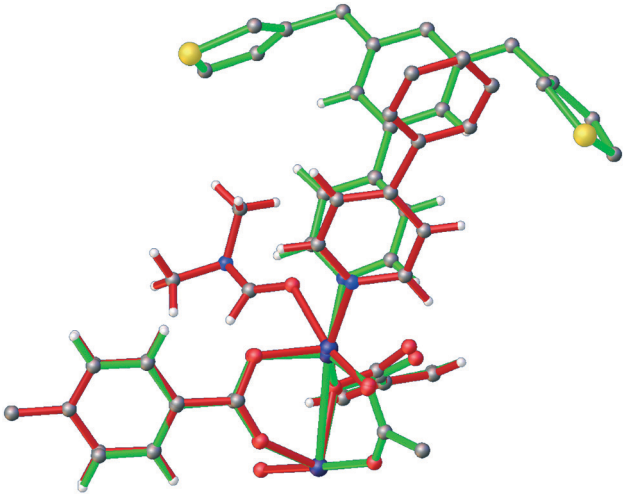

Fig. 4 Overlay of the asymmetric units of **UBMOF-3** (red) and **UBMOF-3a** (green) illustrating the large reorganization upon desolvation. Atom colours: carbon (grey), nitrogen (blue), oxygen (red), sulphur (yellow), zinc (purple) and hydrogen (white).

Table 1 Crystal data and structure refinement for **UBMOF-3** and **UBMOF-3a**

Compound	UBMOF-3	UBMOF-3a
Empirical formula	$C_{101}H_{61.01}N_7O_{27}Zn_6$	$C_{112}H_{48}N_4O_{24}S_4Zn_6$
Formula weight	2196.79	2354.00
Temperature/K	90.0	90.0
Crystal system	Monoclinic	Monoclinic
Space group	*C*2/*c*	*C*2/*c*
a/Å	51.107(13)	39.751(4)
b/Å	9.448(3)	9.7399(11)
c/Å	18.492(5)	18.388(2)
α/°	90	90
β/°	102.189(7)	91.374(4)
γ/°	90	90
Volume/Å^3	8728(4)	7117.1(14)
Z	2	2
ρ_{calc} g cm^{-3}	0.836	1.098
μ/mm^{-1}	0.856	1.109
F(000)	2224.0	2368.0
Crystal size/mm^3	0.1 × 0.05 × 0.01	0.11 × 0.09 × 0.01
Radiation	MoKα (*λ* = 0.71073)	MoKα (*λ* = 0.71073)
2*Θ* range for data collection/°	1.63 to 52.794	4.1 to 52.908
Reflections collected	27 822	28 262
Goodness-of-fit on F^2	1.039	1.087
Final *R* indexes [$I >= 2\sigma(I)$]	R_1 = 0.1054	R_1 = 0.0790
	wR_2 = 0.2852	wR_2 = 0.2163
Final *R* indexes [all data]	R_1 = 0.1527	R_1 = 0.1081
	wR_2 = 0.3082	wR_2 = 0.2305

and the corresponding reduced steric interaction between the **TPDPy** and coordinated solvent. The reorientation of the **TPDPy** linker in **UBMOF-3a** reduces the distance between pendant groups and neighbouring linkers thus increasing intermolecular interactions between these groups (Fig. 4).

Analysis of the packing of the **TPDPy** linkers in both structures reveals that the pillaring linker is a key feature of the structural reorganization upon desolvation (Fig. 5). In **UBMOF-3** prior to desolvation, the long axis of **TPDPy** was nearly parallel to the *a*-axis. Following desolvation in which the length of the *a*-axis is reduced from 51.107 Å to 39.751 Å, the long axis of **TPDPy** reoriented to approximately 45° between the *a*- and *b*-axes. Thus the scissoring of **TPDPy** is likely responsible for the observed structural flexibility in this crystalline framework.

Spectroscopic characterization

Following irradiation with UV light, a decrease in peaks at 225 and 295 nm was noted in the UV-vis spectrum of the free **TPDPy** ligand in methanol, along with the appearance of peaks at 355 and 525 nm (Fig. 6). The peak at 525 nm is responsible for the observed change from colourless to red following irradiation and confirms the photochromic activity of the DAE moiety. The observed spectrum was nearly identical to the previously reported dicarboxylate-phenanthrene DAE linker[26] indicating that substitution of a pyridyl group at the 2,7 positions of the phenanthrene did not result in significant changes in the photophysical properties of the diarylethene portion of the molecule.

The absorbance of **TPDPy** in methanol was monitored at room temperature for 390 minutes following irradiation. A higher concentration was used (2.35×10^{-4} M) to increase the magnitude of the absorbance at 525 nm. As seen in Fig. 6, the absorption band at 525 nm gradually diminished converting the red solution back into a colourless solution. The presence of a thermally activated cycloreversion pathway is another feature shared by the dicarboxylate-phenanthrene linker.[26]

The as-grown (100) plates of **UBMOF-3** were found to be very fragile and did not exceed 15 μm in thickness (10 μm or less being most common). Visible light absorption spectra of single crystals of **UBMOF-3** and **UBMOF-3a** were measured

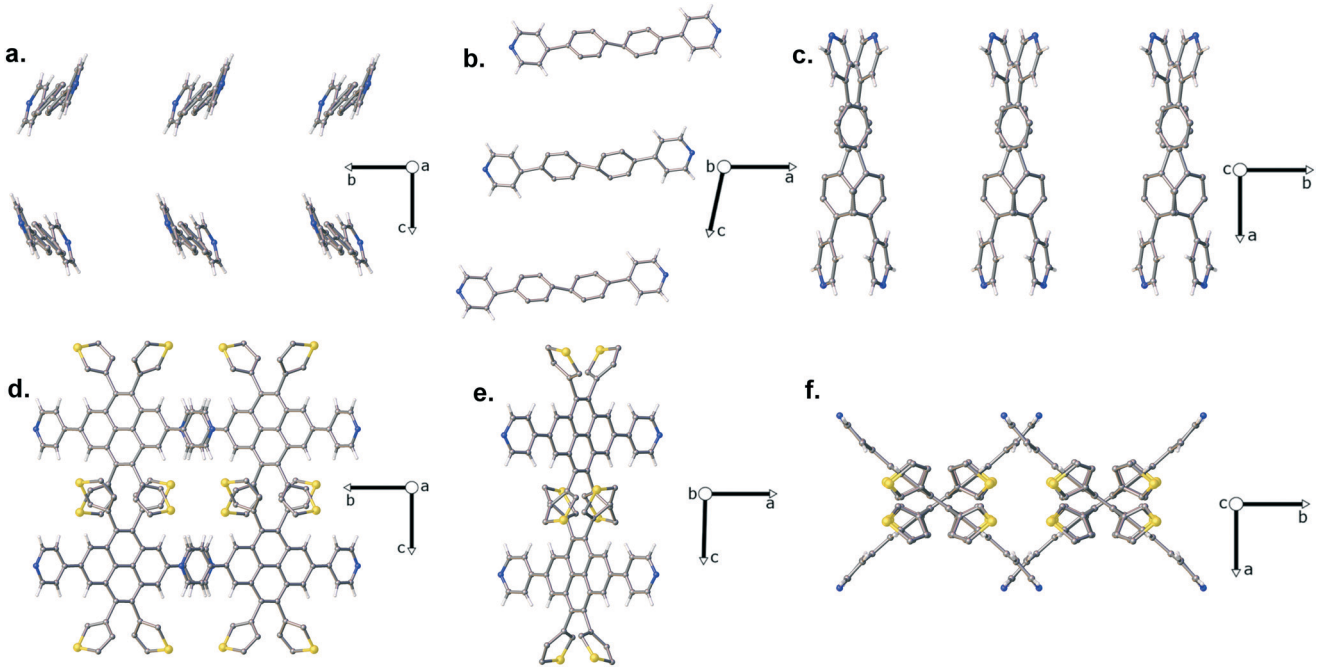

Fig. 5 **TPDPy** linker orientation in the **UBMOF-3** and **UBMOF-3a** crystal structures. **UBMOF-3** along the *a* (a), *b* (b), and *c* (c) axes. **UBMOF-3a** along the *a* (d), *b* (e), and *c* (f) axes. Atom colours: carbon (grey), nitrogen (blue), sulphur (yellow), and hydrogen (white).

normal to (100) prior to and following irradiation with 365 nm light. For both crystals only a modest change in absorption was observed (Fig. S3†). As the long molecular axis (approximately parallel to the electronic transition dipole moment) of the chromophore is nearly parallel to the *a*-axis in **UBMOF-3** and modestly inclined in the case of **UBMOF-3a**, strong absorption was not expected for measurements with light incident on (100). While the crystals were too thin for polarized light measurements perpendicular to (100), we were able to obtain polarized light images of a cut-block of a crystal of **UBMOF-3** (Fig. S4†). These images revealed strong linear dichroism for an irradiated sample viewed perpendicular to (100) that is consistent with the high degree of alignment observed in the crystal structure.

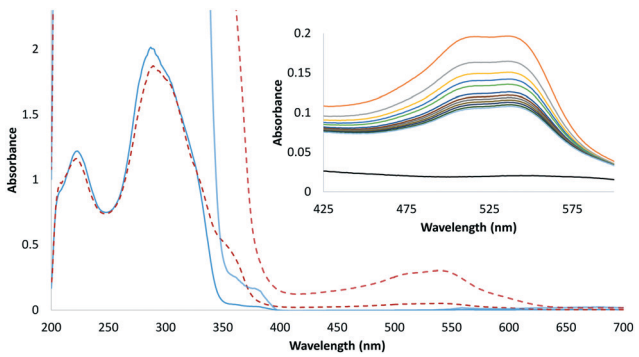

Fig. 6 UV-vis spectra of the **TPDPy** linker in MeOH (9.74×10^{-5} M), lighter trace enlarged for clarity of the absorption band. Inset: Visible region of the spectrum using a higher concentration (2.35×10^{-4} M) prior to irradiation (black) and at the following intervals after irradiation was complete: 0 min (orange), 30 min (grey), 60 min (yellow), 90 min (blue), 120 min (green), 210 min (dark blue), 240 min (brown), 270 min (dark grey), 300 min (tan), 330 min (purple), 360 min (dark green), 390 min (light blue).

Conclusions

A new photo-responsive pyridyl-phenanthrene dithienylethene MOF linker, **TPDPy**, containing pendant photoactive groups has been prepared. The linker exhibits photophysical behaviour similar to a previously synthesized dicarboxylate derivative. An air-stable metal–organic framework, **UBMOF-3**, constructed from this linker exhibits dramatic structural reorganization upon activation. When desolvated, the compressed **UBMOF-3a** lattice results in the improved resolution of the pendant thiophene groups. Absorption spectroscopy revealed the presence of a thermally activated cycloreversion pathway for a neat solution of the pyridyl-phenanthrene linker. The modest spectroscopic response observed in single crystals was attributed to the unfavourable orientation of the photochrome relative to the direction in which optical measurements were performed. Polarized light images of an irradiated single crystal did reveal linear dichroism consistent with the highly aligned linker molecules within the lattice.

Acknowledgements

This material is based upon work supported by the National Science Foundation under Grant No. DMR-1455039.

Notes and references

1 D. M. D'Alessandro, B. Smit and J. R. Long, *Angew. Chem., Int. Ed.*, 2010, **49**, 6058–6082.

2 J. A. Mason, M. Veenstra and J. R. Long, *Chem. Sci.*, 2014, **5**, 32–51.
3 Z. Zhang, H. T. H. Nguyen, S. A. Miller, A. M. Ploskonka, J. B. DeCoste and S. M. Cohen, *J. Am. Chem. Soc.*, 2016, **138**, 920–925.
4 K. Eum, K. C. Jayachandrababu, F. Rashidi, K. Zhang, J. Leisen, S. Graham, R. P. Lively, R. R. Chance, D. S. Sholl, C. W. Jones and S. Nair, *J. Am. Chem. Soc.*, 2015, **137**, 4191–4197.
5 S. A. Kumalah Robinson, M.-V. L. Mempin, A. J. Cairns and K. T. Holman, *J. Am. Chem. Soc.*, 2011, **133**, 1634–1637.
6 S. Rojas, F. J. Carmona, C. R. Maldonado, P. Horcajada, T. Hidalgo, C. Serre, J. A. Navarro and E. Barea, *Inorg. Chem.*, 2016, **55**, 2650–2663.
7 H.-Y. Li, Y.-L. Wei, X.-Y. Dong, S.-Q. Zang and T. C. W. Mak, *Chem. Mater.*, 2015, **27**, 1327–1331.
8 S.-Y. Moon, A. J. Howarth, T. Wang, N. A. Vermeulen, J. T. Hupp and O. K. Farha, *Chem. Commun.*, 2016, **52**, 3438–3441.
9 C. F. Leong, T. B. Faust, P. Turner, P. M. Usov, C. J. Kepert, R. Babarao, A. W. Thornton and D. M. D'Alessandro, *Dalton Trans.*, 2013, **42**, 9831–9839.
10 L. M. Lifshits, B. C. Noll and J. K. Klosterman, *Chem. Commun.*, 2015, **51**, 11603–11606.
11 S. S. Nagarkar, A. V. Desai and S. K. Ghosh, *Chem. – Asian J.*, 2014, **9**, 2358–2376.
12 F.-X. Coudert, *Chem. Mater.*, 2015, **27**, 1905–1916.
13 J. W. Brown, B. L. Henderson, M. D. Kiesz, A. C. Whalley, W. Morris, S. Grunder, H. Deng, H. Furukawa, J. I. Zink, J. F. Stoddart and O. M. Yaghi, *Chem. Sci.*, 2013, **4**, 2858–2864.
14 C. L. Jones, A. J. Tansell and T. L. Easun, *J. Mater. Chem. A*, 2016, **4**, 6714–6723.
15 S. Castellanos, F. Kapteijn and J. Gascon, *CrystEngComm*, 2016, **18**, 4006–4012.
16 A. Priimagi, C. J. Barrett and A. Shishido, *J. Mater. Chem. C*, 2014, **2**, 7155–7162.
17 T. J. Kucharski, Y. Tian, S. Akbulatov and R. Boulatov, *Energy Environ. Sci.*, 2011, **4**, 4449–4472.
18 W. Wu, J. Wang, Z. Zheng, Y. Hu, J. Jin, Q. Zhang and J. Hua, *Sci. Rep.*, 2015, **5**, 8592.
19 R. Castagna, M. Garbugli, A. Bianco, S. Perissinotto, G. Pariani, C. Bertarelli and G. Lanzani, *J. Phys. Chem. Lett.*, 2012, **3**, 51–57.
20 M. Cacciarini, A. B. Skov, M. Jevric, A. S. Hansen, J. Elm, H. G. Kjaergaard, K. V. Mikkelsen and M. Brøndsted Nielsen, *Chem. – Eur. J.*, 2015, **21**, 7454–7461.
21 J. I. Feldblyum, E. A. Keenan, A. J. Matzger and S. Maldonado, *J. Phys. Chem. C*, 2012, **116**, 3112–3121.
22 S. Castellanos, A. Goulet-Hanssens, F. Zhao, A. Dikhtiarenko, A. Pustovarenko, S. Hecht, J. Gascon, F. Kapteijn and D. Bléger, *Chem. – Eur. J.*, 2016, **22**, 746–752.
23 A. Modrow, D. Zargarani, R. Herges and N. Stock, *Dalton Trans.*, 2011, **40**, 4217–4222.
24 S. Bernt, M. Feyand, A. Modrow, J. Wack, J. Senker and N. Stock, *Eur. J. Inorg. Chem.*, 2011, **2011**, 5378–5383.
25 F. Luo, C. B. Fan, M. B. Luo, X. L. Wu, Y. Zhu, S. Z. Pu, W.-Y. Xu and G.-C. Guo, *Angew. Chem., Int. Ed.*, 2014, **53**, 9298–9301.
26 D. G. D. Patel, I. M. Walton, J. M. Cox, C. J. Gleason, D. R. Butzer and J. B. Benedict, *Chem. Commun.*, 2014, **50**, 2653–2656.
27 J. Park, D. Feng, S. Yuan and H.-C. Zhou, *Angew. Chem., Int. Ed.*, 2015, **54**, 430–435.
28 I. M. Walton, J. M. Cox, C. A. Benson, D. G. Patel, Y.-S. Chen and J. B. Benedict, *New J. Chem.*, 2016, **40**, 101–106.
29 H. Li, M. Eddaoudi, M. O'Keeffe and O. M. Yaghi, *Nature*, 1999, **402**, 276–279.
30 O. V. Dolomanov, L. J. Bourhis, R. J. Gildea, J. A. K. Howard and H. Puschmann, *J. Appl. Crystallogr.*, 2009, **42**, 339–341.
31 G. Sheldrick, *Acta Crystallogr., Sect. A: Found. Crystallogr.*, 2008, **64**, 112–122.
32 G. M. Sheldrick, *Acta Crystallogr., Sect. C: Struct. Chem.*, 2015, **71**, 3–8.
33 M. J. Frisch, *et al.*, *Gaussian 09*, Gaussian, Inc., 2009.
34 J.-D. Chai and M. Head-Gordon, *Phys. Chem. Chem. Phys.*, 2008, **10**, 6615–6620.
35 D. E. Williams, J. A. Rietman, J. M. Maier, R. Tan, A. B. Greytak, M. D. Smith, J. A. Krause and N. B. Shustova, *J. Am. Chem. Soc.*, 2014, **136**, 11886–11889.
36 J. M. Cox, I. M. Walton and J. B. Benedict, *J. Mater. Chem. C*, 2016, **4**, 4028–4033.
37 S. Kobatake, K. Uchida, E. Tsuchida and M. Irie, *Chem. Commun.*, 2002, 2804–2805.
38 Y.-L. Liu, K.-F. Yue, B.-H. Shan, L.-L. Xu, C.-J. Wang and Y.-Y. Wang, *Inorg. Chem. Commun.*, 2012, **17**, 30–33.